DETECTION OF THE GEOTHERMAL ALTERATIONS AND THERMAL ANOMALIES BY PROCESSING OF REMOTE SENSING DATA, SABALAN, IRAN

Tohid NOURI, Majid Mohammady Oskouei

Sahand University of Technology, Tabriz, Iran, Tel:+984123459299
Email: t_nouri@sut.ac.ir, mohammady@sut.ac.ir

KEYWORDS: ASTER, linear spectral unmixing, geothermal, hydrothermal alteration, thermal anomaly.

Abstract: Geothermal energy is directly related to radioactive elements inside of the earth. In geothermal areas thermal gradient is higher than vicinity regions. Extraction of thermal energy is therefore more beneficial in these areas. The Sabalan, Damavand, Sahand, Taftan, and Bazman regions have been proved as good potentials for geothermal energy in Iran. This study aims assessment of capability of remote sensing technology for detection of geothermal resources in Sabalan geothermal area. To do this task, processing of two datasets of Advanced Spaceborn Thermal Emission and Reflection radiometer (ASTER) data were used for alteration detection. Two ASTER scenes from the study area were therefore merged and processed. The applied method for mineral detection in this research is linear spectral unmixing. The important alterations (carbonate, borate, iron oxides, and clay minerals) were successfully detected and mapped. Besides that, the thermal anomalies were also investigated and mapped with the use of ASTER thermal channels. The resultant maps were then validated with comparing to the results of geophysical surveys available from SUNA organization. According to their works, the anomaly maps resulted from ASTAR data processing are able to illuminate the geothermal potential in the study area.

INTRODUCTION

Geothermal energy originates from collapsing of existing radioactive elements inside of the earth. In geothermal areas this source of heat energy, in the form of magma, is closer to the surface than other places. This kind of energy is one of the clean energy types and could be used directly for electricity generating. Detection of geothermal resources, therefore, has been much of interest for earth scientists. Considering the alteration caused by magma and hydrothermal fluids in surrounding rocks particularly around faults and fractures, a diversity of geochemical methods have been applied to geothermal resources explorations. Sinters, the chemical precipitates of hydrothermal systems, generally consist of mineral dominated by silica, carbonate, borates, metallic sulfides and oxides, and clay minerals (Hellman etal. 2004, Coolbaugh etal. 2006, Kratt etal. 2006). Therefore, areas that show anomalies of above mentioned minerals will be good targets for planning more detail exploration. Detection of such regions can be easily done by processing of remote sensing data. Exploration of Geothermal energy with remote sensing technology is useful in the early stages of exploration (Fernández etal. 2001). For a long time, geological remote sensing researchers have focused on the use of spectral signatures for rock type discrimination and mineral mapping, especially hydrothermal alteration minerals (Rowan etal. 2003). The use of remote sensing data analysis for geothermal exploration has been investigated in previous researches (e.g Coolbaugh etal. 2006,2007, Kratt etal. 2006,2009,2010, Eneva etal. 2007,2009).

Recent developments in processing of both multi and hyperspectral data have led to the extensive application of those data in mineral detection. ASTER is one of the spaceborn multispectral satellite imagery systems that have been used for mineral exploration and it has better spectral resolution both in SWIR and thermal regions comparing to LANDSAT imagery (Azizi etal. 2010). As a result, on the basis of spectral characteristics of minerals, different alteration minerals are detected and mapped using ASTER data (Tangestani etal. 2008). Because of vicinity of geothermal systems to land surface, detection of geothermal related thermal anomalies could be another technique for underground geothermal systems exploration and thermal channels of ASTER data are also applied for surface temperature assessments and analysis.

In this study, surface indicators (alteration minerals and thermal anomalies) of geothermal resources in Sabalan Mountain were detected. To do this task, the clay minerals, silica, borates, carbonates, and iron oxides were selected as indicator. Spectral image processing techniques including endmembers detection and unmixing algorithm were performed on the ASTER data. Finally we processed thermal bands of ASTER for extraction of geothermal related surface thermal anomalies.

DATA ACQUISITION AND PREPROCESSING

In this study two georeferenced scenes of ASTER level 1B data were merged to achieve necessary coverage of the region. In figure 1 time of acquisition and position of data is illustrated. The data was then atmospherically and topographically corrected using FLAASH and Lambertian (Riaño etal. 2003) method respectively before running the unmixing and thermal procedures.

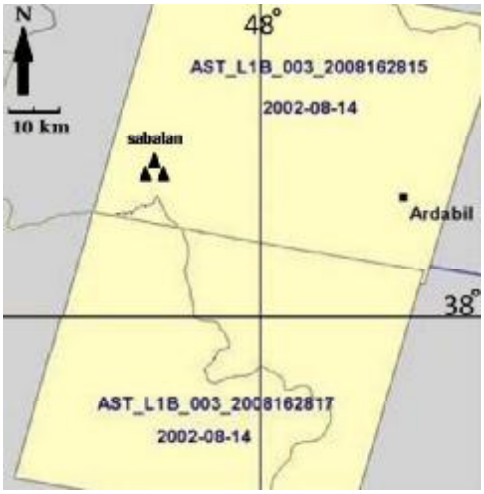

Figure 1: position and time of acquisition the ASTER data.

LINEAR SPECTRAL UNMIXING ALGORITHM (LSU)

In this study geothermal related minerals were detected using unmixing algorithm. In LSU algorithm, as indicated in equation 1, an unknown pixel usually consisted of different materials and the total reflection of a pixel is considered as a linear mixings of reflections of the materials (Chang. 2007, Borengasser etal. 2008) where X is pixel spectrum, a_i is coefficient of i^{th} reference spectrum (endmember), s_i is i^{th} reference spectrum, and w is noise. Unmixing algorithm determines contribution of different materials in all pixels of data with decomposition of their spectrums. Before implementation of Unmixing algorithm four steps needs to be done including: 1) minimum noise fraction (MNF), 2) pixel purity index (PPI), 3) n-dimensional visualization (n-DV), 4) spectral analysis.

$$x = \sum_{i=1}^{M} a_i s_i + w = Sa + w \quad (1)$$

MINIMUM NOISE FRACTION (MNF)

MNF is statistical method similar to PCA (Azizi etal. 2010) that separates noise from data and gives estimation about actual dimensionality of data and reduces latter computations. After preprocessing, the MNF algorithm was implemented for noise whitening and preparing the data for Pixel Purity Index (PPI). In the MNF derived image there is no correlation among bands and its first band reflects main part of information, as indicated in the figure 2 due to its higher eigenvalue comparing to following bands (figure 3).

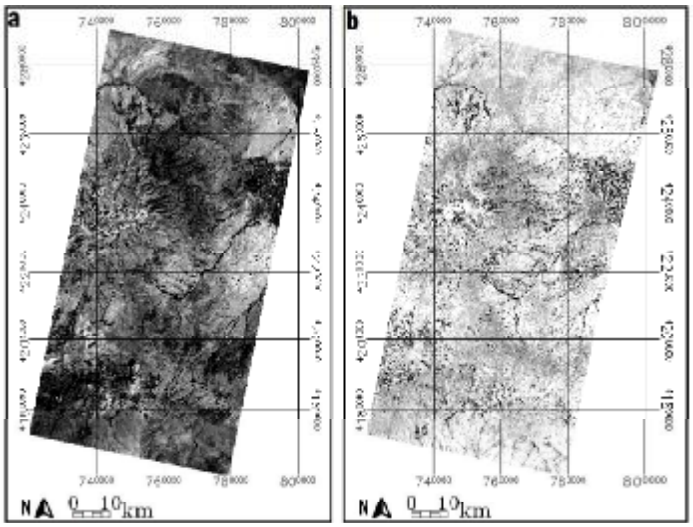

Figure 2: MNF image of the study area. (a) band. 1 and (b) band. 2.

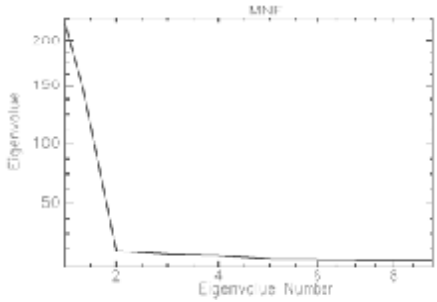

Figure 3: Eigenvalues of MNF image bands 1 to 9

PIXEL PURITY INDEX (PPI)

Recently many algorithms were developed for extraction of pure pixels of remote sensing multi and hyperspectral data and PPI is one of efficient algorithms for this task. PPI is the method that determines relative purity of pixels using the convex geometry argument (Qiu etal. 2006). In the PPI algorithm n random unit vectors are generated in m-dimensional data space (m is the number of MNF image bands in this case) and all pixels are projected to these random vectors. After predefined iterations, pixels that their projections fall far from mean projection by a certain threshold are marked as pure pixels. PPI algorithm was therefore implemented over MNF image for detection of purest pixels. Most of the pure pixels of the study area are in the western and eastern parts as indicated in figure 4.

N-DIMENSIONAL VISUALIZATION

In the PPI algorithm pixels are evaluated in terms of purity and characteristics of pure pixels are not recognized. They were plotted in an n-dimensional space for grouping of pure pixels. This is done by ENVI's N-Dimensional Visulizer and 5 classes were detected by visual interpretation (Figure 5). For determination of mineralogy of detected classes the mean spectrum of each of them were calculated.

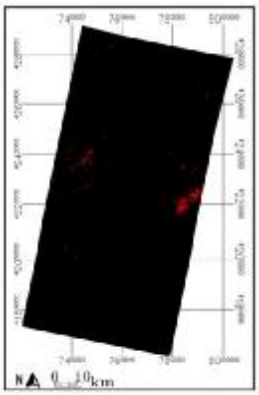

Figure 4: Pure pixels of the study area (red pixels).

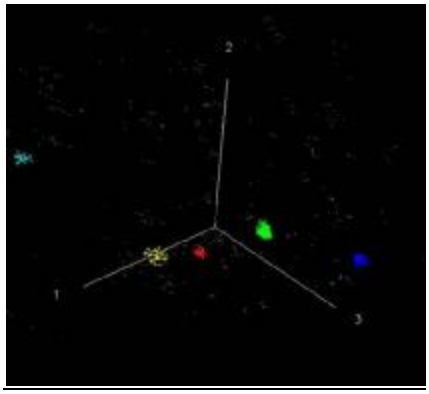

Figure 5: clouds of pure pixels in 3D view and 5 distinguished classes.

SPECTRAL ANALYSIS

Spectral analysis is used to identify different mineral types based on their spectral features (Qiu etal. 2006). The spectral analysis was applied for determination of mean spectrums (endmembers) using Spectral Angle Mapper (SAM), Spectral Feature Fitting (SFF), and Binary Encoding (BE) algorithms and USGS mineral spectral library as references spectra. To do this task, the reference library was resampled according to ASTER channels (figure 6). Finally the minerals of the spectral library having higher matching score to the endmembers based on the total scores of the three comparison methods were selected. The matching of absorption features on the reference and endmembers spectral profile were then visually checked to select best matches to the endmembers. The minerals Calcite, Montmorillonite, Tincalconite, Silica, and Hematite were therefore detected as representatives of 5 classes (table 1, figure 7).

Table 1: assigned minerals to the detected classes.

Class No	Mineral type	SAM	SFF	BE
Class1	**Calcite**	**0.902**	**0.704**	**0.778**
Class2	**Montmorillonite**	**0.865**	**0.843**	**0.889**
Class3	**Tincalconite**	**0.929**	**0.692**	**0.889**
Class4	**Quartz**	**0.814**	**0.763**	**0.778**
Class5	**Hematite**	**0.888**	**0.990**	**0.889**

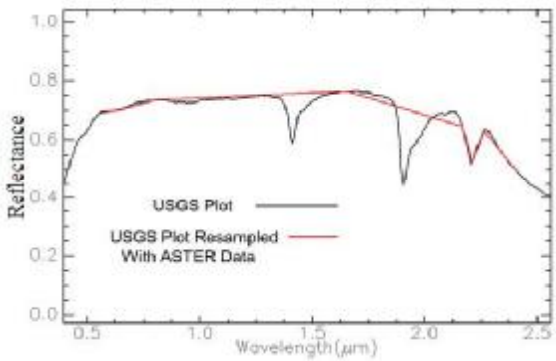

Figure 6: resampled montmorillonite and its original spectral profile.

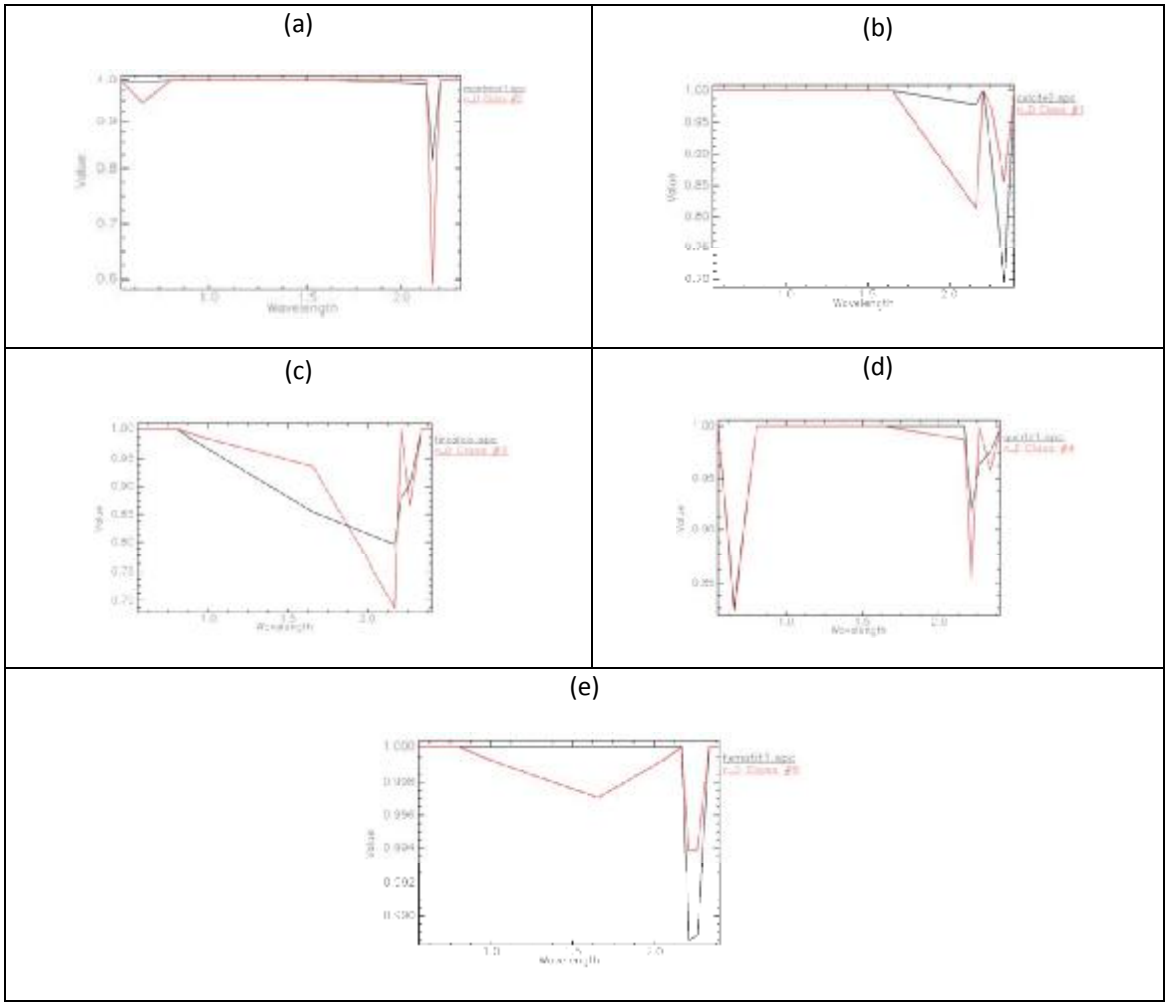

Figure 7: absorption features of the mean spectrum of 5 classes (red lines) and their best fit from library (black lines). (a) montmorillonite (b) calcite (c) tincalconite (d) quartz (e) hematite.

After detection of endmembers, LSU algorithm was applied for computing of the abundances of detected minerals. The results were then integrated by rule classifier algorithm to achieve minerals distribution map. Each pixel was therefore assigned to one of the detected endmembers if its contribution in that pixel had been more than predefined thresholds. The abundance map of detected minerals was illustrated in figure 8.

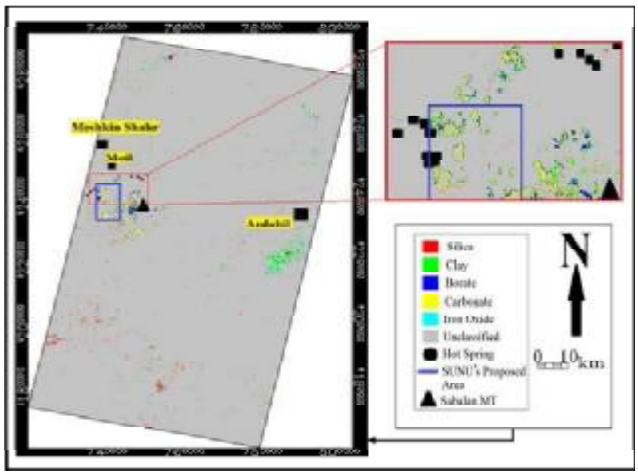

Figure 8: abundance map of detected minerals image

THERMAL ANOMALY EXTRACTION

Detection of thermal anomalies is really helpful for geothermal exploration since it directly reflects the presence of thermal sources. For achieving a temperature anomaly map of the study area we applied the 13th band of ASTER data for extraction of Brightness Temperature (BT) explained by (Zhang etal. 2008). Extraction of BT image from radiance based images such as ASTER 13th band was done by equation (2) where T_c is BT (^{o}k), c_1=1.191×10^{8}w/(m^2×sr×μm), c_2=1.439×10^{4}μm×k, and λ_c is the wavelength in μm. As indicated in figure 9, the BT image was obscure because of the high variation in the area elevation.

$$T_c = \frac{c_2}{\lambda_c Ln\left(\frac{c_1}{\lambda_c^5.(L_S+1)}\right)} \quad (2)$$

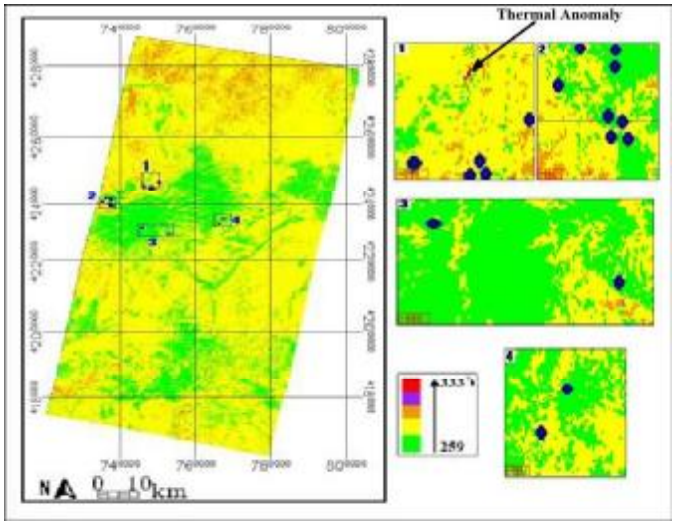

Figure 9: BT image of 13th band of ASTER data.

If other effective parameters are constant, land surface temperature (LST) decreases by increasing of area elevation with rate of –6.5^{o}C/km (Eneva etal. 2009). Inverse relationship between elevation and LST in the study area is indicated in figure 10. To improve the temperature map, we performed the elevation effect correction with the use of Digital Elevation Model (DEM) of the region (figure 10a) and equation (3) where T_H is BT of each pixel after elevation correction and H is elevation (m). In the corrected map the north-western part of the Sabalan MT, containing youngest intrusive of the study area and hot springs, shows an obvious thermal anomaly (figure 11) and the highest thermal anomalies (red pixels) are closed to hot springs.

$$T_H = T_c + 0.0065\,H \quad (3)$$

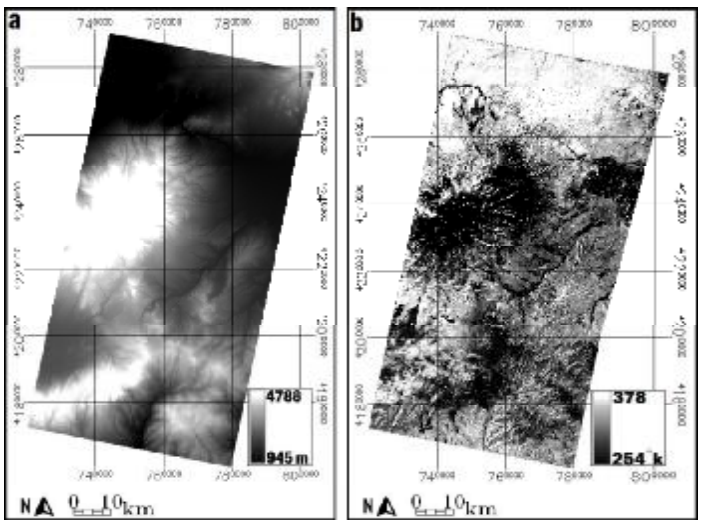

Figure 10: (a) Digital elevation model. (b) ASTER band 13 image. There is inverse relationship between temperature and elevation.

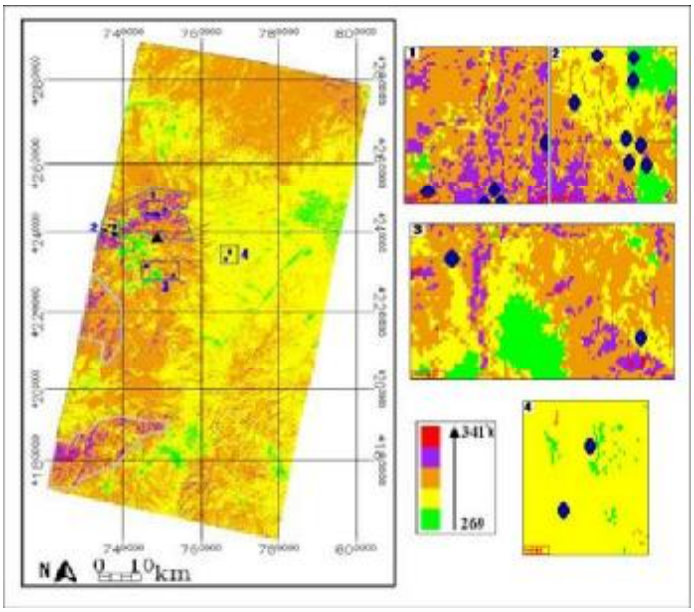

Figure 11: The temperature anomaly map.

RESULTS AND DISCUSSION

Prior to this study, a geothermal exploration project had been accomplished by SUNA organization in the Movil area in north western of the Sabalan Mountains using field studies (geochemical and geophysical methods) (Eshaghpour. 2005, Talebi etal. 2005, Noorollahi etal. 2003, Bogie etal. 2005). In this research hydrothermal alteration related minerals including iron oxides, silica, clay, carbonate, and borate were detected in the SUNA study area, northwestern of Sabalan MT and there is a high conformity between the results of this study and the proposed area by SUNA. Therefore, other anomalies detected in this research (southern of Ardabil and other promising areas marked on the map (Figure 11)) can be considered as promising targets for detail field studies. The chemical analysis of hot springs of Sabalan region indicates significant amounts of dissolved Boron and Carbonate in some of their composition such as Ghaynarjeh and we detected these minerals near the hot springs with the use of unmixing algorithm (Figure 8). This is another evidence for reliability of the applied method. BT image indicates an extensive thermal anomaly in the north western part of Sabalan MT where wide hydrothermal alteration exists. However an extensive alteration, has been detected in the western part of study area, southern of Ardabil city, is not associated with high temperatures in corresponding thermal image, this area is promising for detail field studies because often large aquifers conceal thermal anomalies in the surface (Ardabil Plane Aquifer in this area).

REFERENCES

Azizi, H., Tarverdi, M.A., Akbarpour, A., 2010a. Extraction of hydrothermal alterations from ASTER SWIR data from east Zanjan, northern Iran. Advances in Space Research, 46, 99–109.

Bogie, I., Khosrawi, Kh., Talebi, B., 2005b. Geological Results from the Drilling of the Northwest Sabalan Geothermal Project, Iran. Proceedings World Geothermal Congress, Antalya, Turkey, 24-29 April 2005.

Borengasser, M., Hungate, W.S., Watkins, R., 2008. Hyperspectral Remote Sensing, Principles and Applications.

Chang, Ch., 2007. Hyperspectral data exploitation, theory and applications, University of Maryland, Baltimore County, Baltimore, MD.

Coolbaugh, M.F., Kratt, C., Fallacaro, A., Calvin, W.M., Taranik, J.V., 2007a. Detection of geothermal anomalies using Advanced Spaceborne Thermal Emission and Reflection Radiometer (ASTER)

thermal infrared images at Bradys Hot Springs, Nevada, USA. Remote Sensing of Environment, 106, 350–359.

Coolbaugh, M.F., Kratt, Ch., Sladek, Ch., Zehner, R.E., Shevenell, L., 2006a. Quaternary Borate Deposits as a Geothermal Exploration Tool in the Great Basin. GRC Transactions, Vol. 30.

Eneva, M., Coolbaugh, M., Steven C.B., Combs, J., 2007b. In search for thermal anomalies in the Coso Geothermal Field (California) using remote sensing and field data. proceedings, Thirty-Second Workshop on Geothermal Reservoir Engineering, Stanford University, Stanford, California, January 22-24, SGP-TR-183.

Eshaghpour, M., 2005b. Borehole Geology and Alteration Mineralogy of Well NWS-4, Mt.Sabalan Geothermal Field, NW-Iran. Proceedings World Geothermal Congress, Antalya, Turkey, 24-29 April 2005.

Fernández de la Vega-Márquez, T., Prol-Ledesma, R.M., Orozco, G., 2001a. Hydrothermal alteration and main structures mapping using TM images in La Primavera geothermal field (Mexico). Geofísica Internacional, Vol. 40, Num. 3, pp. 147-162.

Hellman, M.J., Ramsey, M. S., 2004a. Analysis of hot springs and associated deposits in Yellowstone national park using ASTER and AVIRIS remote sensing. Journal of volcanology and geothermal research, 135, 195– 219.

Kratt, Ch., Calvin, W.M., Coolbaugh, M., 2010a. Mineral mapping in the Pyramid Lake basin: Hydrothermal alteration, chemical precipitates and geothermal energy potential. Remote Sensing of Environment 114, 2297–2304.

Kratt, Ch., Coolbaugh, M., Peppin, B., Sladek, Ch., 2009a. Identifcation of a new blind geothermal system with hyperspectral remote sensing and shallow temperature measurements at columbus salt marsh, esmeralda county, Nevada. GRC Transactions, Vol. 33.

Kratt, Ch., Coolbaugh, M., Calvin, W., 2006a. Remote detection of quaternary borate deposits with ASTER satellite imagery as a geothermal exploration tool. GRC Transactions, Vol. 30.

Noorollahi, Y., Yousefi, H., 2003b. Preliminary environmental impact assessment of a geothermal project in Meshkinshahr, NW-Iran. International Geothermal Conference, Reykjavík, Sept 2003.

Qiu, F., Abdelsalam, M., Thakkar, P., 2006a. Spectral analysis of ASTER data covering part of the Neoproterozoic Allaqi-Heiani suture, Southern Egypt. Journal of African Earth Sciences, 44, 169–180.

Rowan L.C., Mars, J.C., 2003a. Lithologic mapping in the Mountain Pass, California area using Advanced Spaceborne Thermal Emission and Reflection Radiometer (ASTER) data, Remote Sensing of Environment, 84(2003)350–366.

Talebi, B., Khosrawi, Kh., Ussher, G., 2005b. Review of Resistivity Surveys from the NW Sabalan Geothermal Field, Iran. Proceedings World Geothermal Congress, Antalya, Turkey, 24-29 April 2005.

Tangestani, M.H., Hosseinjani, M., 2008b. Spectral Angle Mapping and Linear Spectral Unmixing of the ASTER data for alteration mapping at Sarduiyeh area, SE Kerman, Iran. MWF09 PN-164.

Zhang, G., Liu, J., Fei, W., 2008b. Detection of Anomaly Temperature Based on ASTER and ETM+ Thermal Infrared Image. International conference on computer science and software engineering.

Riaño, D., 2003a. Assessment of Different Topographic Corrections in Landsat-TM Data for Mapping Vegetation Types. IEEE transactions on geoscience and remote sensing, 41(5), pp.1056-1061.

Eneva, M., Coolbaugh, M., 2009b. Importance of elevation and temperature inversions for the interpretation of thermal infrared satellite images used in geothermal exploration.